International Journal of Heat and Mass Transfer 52 (2009) 3757–3766

Contents lists available at ScienceDirect

International Journal of Heat and Mass Transfer

journal homepage: www.elsevier.com/locate/ijhmt

Evaluation of the different definitions of the convective mass transfer coefficient for water evaporation into air

H.-J. Steeman [a,*], C. T'Joen [a], M. Van Belleghem [a], A. Janssens [b], M. De Paepe [a]

[a] Department of Flow, Heat and Combustion Mechanics, Ghent University – UGent, Sint-Pietersnieuwstraat 41, 9000 Gent, Belgium
[b] Department of Architecture and Urbanism, Ghent University – UGent, Jozef Plateaustraat 22, 9000 Gent, Belgium

ARTICLE INFO

Article history:
Received 18 August 2008
Accepted 2 January 2009
Available online 6 April 2009

Keywords:
Convective mass transfer coefficient
Evaporation
CFD
Heat and mass analogy

ABSTRACT

In literature different definitions of the convective mass transfer coefficient are used by different authors. The definitions differ in the driving force used to describe mass transfer. In this paper, the limitations to the use of convective mass transfer coefficients related to four commonly used driving forces (vapour density, mass fraction, vapour pressure and mole fraction) are studied for evaporation of water into air. A theoretical study based on the adiabatic saturation process and a numerical CFD study of an existing evaporation experiment show that the use of convective mass transfer coefficients related to vapour densities is only allowed under isothermal conditions while convective mass transfer coefficients related to vapour pressure show a dependence on the total gas pressure. The use of mole or mass fractions as driving force results in values for the transfer coefficient which are little affected by the thermodynamic properties such as temperature, relative humidity and total pressure and are hence better suited to describe convective mass transport.

1. Introduction

Mass transfer at the interface between a liquid or solid and a gas is an important phenomenon for various engineering disciplines. The mass transfer rate at these interfaces is often described using a convective mass transfer coefficient. Analogous to the convective heat transfer coefficient, the convective mass transfer coefficient can be used to calculate the mass transfer rate by multiplying it with a driving force and the area of the considered surface. Depending on the author and on the scientific discipline different choices have been made to define the mass transfer coefficient and the related driving force.

If we consider the research on evaporation and on moisture transfer to porous materials, already two different driving forces for convective mass transfer are commonly used: on the one hand the difference between the vapour density at the interface and in the gas free stream is used [1–4] and on the other hand the difference in mass fractions is used as the driving force [5–8]. In building engineering it is common practise to use the difference in vapour pressure as a driving force for mass transfer, and also in other disciplines this choice is sometimes made [9–13]. The last possibility considered in this paper to express the driving force is the use of mole fractions (or ratio of vapour pressure and total pressure) [14].

Numerous studies have been performed to determine correlations for mass transfer coefficients (or Sherwood numbers) for different geometries, flow regimes and applications [1,12,15–17]. The practical use of such correlations could be strongly improved if they could also be applied under different ambient conditions. The issue with varying ambient conditions such as temperature is that this can lead to a change in buoyancy forces and hence a change in flow regime, which results in a change of the governing correlation (e.g. [17]). The varying ambient conditions can also affect the material properties necessary to describe the heat and mass transfer process. Boukakdida studied the effect of a variation in free stream conditions on the mass transfer coefficient for an evaporation case and stated that the evolution of the mass transfer coefficient with the investigated variables changes when another driving force is used to define the mass transfer coefficient [15]. The question which is raised now is whether the dependency of the mass transfer coefficient on the ambient (free stream and surface) conditions is entirely due to changing flow regimes and material properties or whether it in some cases is an artefact of the driving force used. In other words are all the different definitions of the mass transfer coefficient valid when describing convective mass transfer under changing ambient conditions?

Hence the aim of this study is to evaluate if all the above mentioned definitions for the convective mass transfer coefficient are equally suited to accurately describe convective mass transfer. If this is not the case, the limitations of the different definitions will be investigated.

* Corresponding author. Tel.: +32 9 264 3289; fax: +32 9 264 3575.
E-mail address: hendrikjan.steeman@ugent.be (H.-J. Steeman).

0017-9310/$ - see front matter © 2009 Elsevier Ltd. All rights reserved.
doi:10.1016/j.ijheatmasstransfer.2009.01.047

Nomenclature

ΔH_L	latent heat of vaporization (J/kg)
A	area of evaporating surface (m^2)
c	molar concentration (mol/m^3)
Cp	heat capacity (J/kgK)
D	mass diffusion coefficient (m^2/s)
D_H	hydraulic diameter (m)
g	convective mass flux (kg/m^2s)
G	convective mass flow (kg/s)
Gr	Grashof number
Gz	Graetz number
h	convective heat transfer coefficient (W/m^2K)
h_m	convective mass transfer coefficient
Le	Lewis number, $Le = Sc/Pr$
$\dot{m}$	mass flow rate (kg/s)
M	molar weight (kg/mol)
$\dot{n}$	molar flow rate (mol/s)
n	normal direction (m)
Nu	Nusselt number, $Nu = hD_H/\lambda$
P	pressure (Pa)
Pr	Prandtl number, $Pr = \mu/\rho\alpha$
Q	convective heat flow (W)
R	specific gas constant (J/kgK)
Ra	Rayleigh number for mass transfer, $Ra = GrSc$
Re	Reynolds number, $Re = \rho v D_H/\mu$
Sc	Schmidt number, $Sc = \mu/\rho D$
Sh	Sherwood number, $Sh = h_m{}^{\rho} D_H/D = h_m{}^{Y} D_H/\rho D$
T	temperature (K)
v	velocity (m/s)
x	axial length (m)
x^*	dimensionless axial length (–)
Y	mass fraction (kg/kg)
Z	mole fraction (mol/mol)

Greek symbols

α	thermal diffusivity (m^2/s)
λ	thermal conductivity (W/mK)
ρ	density (kg/m^3)

Subscripts

∞	free stream
a	air
in	inlet
m	mean condition
out	outlet
s	surface
sat	saturation
v	water vapour
wet	wet bulb
x	local condition

Superscripts

P	pressure as driving force
ρ	density as driving force
Y	mass fraction as driving force
Z	mole fraction as driving force

The analysis conducted in this paper consists of two parts. Firstly the behaviour of the different driving forces for mass transport is investigated based on theoretical considerations (the conservation of mass, energy and momentum). The different definitions of the convective mass transfer coefficient are also applied to the theoretical case of an adiabatic saturation process. This allows to determine the validity of the different definitions for the convective mass transfer coefficient. In the second part of the paper a CFD (Computational Fluid Dynamics) study of an existing evaporation experiment [1] is executed. The CFD study demonstrates the effect of the improper use of convective mass transfer coefficients.

2. Theoretical considerations about the choice of the driving force for mass transport

2.1. Governing equations for mass transfer

When studying convective mass transfer coefficients related to different driving forces it is very useful to write down the governing mass transport equations at the interface between the gas and the liquid or solid. Under the condition that Fick's law of diffusion is valid and the interface is semi-permeable, the mass flux can be expressed by the following equations:

$$h_m^{\rho}(\rho_{v,s} - \rho_{v,\infty}) = g = -\frac{D}{1-Y_s}\frac{d\rho_v}{dn}\bigg|_{n=0} \quad (1)$$

$$h_m^{Y}(Y_s - Y_{\infty}) = g = -\frac{\rho D}{1-Y_s}\frac{dY}{dn}\bigg|_{n=0} \quad (2)$$

$$h_m^{P}(P_{v,s} - P_{v,\infty}) = g = -\frac{1}{R_v T}\frac{D}{1-Z_s}\frac{dP_v}{dn}\bigg|_{n=0} \quad (3)$$

$$h_m^{Z}(Z_s - Z_{\infty}) = g = -\frac{P}{R_v T}\frac{D}{1-Z_s}\frac{dZ}{dn}\bigg|_{n=0} \quad (4)$$

The above equations represent four alternatives to express mass transfer at a surface by using vapour density (Eq. (1)), mass fraction (Eq. (2)), vapour pressure (Eq. (3)) and mole fraction (Eq. (4)) as driving force. The factor $1/(1-Y_s)$ or $1/(1-Z_s)$ in the right hand side of these equations represents the effect of the semi-permeable surface: as only one species can penetrate the surface, the diffusion flux of a species A is not accompanied by a diffusion of species B in the opposite direction, which results in a net fluid flow. Hence diffusion over a semi-permeable surface is always accompanied by convection. More information about this phenomenon and the derivation of the factor $1/(1-Y_s)$ can be found in [9,18]. In the process of water evaporation into air the water surface can be considered semi-permeable.

The right hand side of Eqs. (1)–(4) shows that the mass flux at the surface is induced by diffusion and the resulting convection flow. However, not all driving forces are equally suited to describe the diffusion process. According to heat and mass transfer handbooks (e.g. [18,19]), Eq. (1) is a simplification of Eq. (2) which is only valid under isothermal and isobaric conditions (thus under constant density). Eq. (3) is a simplification of Eq. (4), valid for isobaric conditions. Due to these limitations the choice is made in this paper to use mass fraction gradients to calculate the diffusive mass fluxes at the surface.

2.2. Performance of different parameters indicating mixture composition

To better understand the limitations of the different parameters indicating mixture composition the example of humid air passing through a heated channel is discussed (Fig. 1). Inside the channel only heat is added, no moisture is added or removed. Hence the composition of the mixture at the outlet of the channel is the same as at the inlet. By consequence, a good definition of the driving force for mass transport should result in a value of zero between

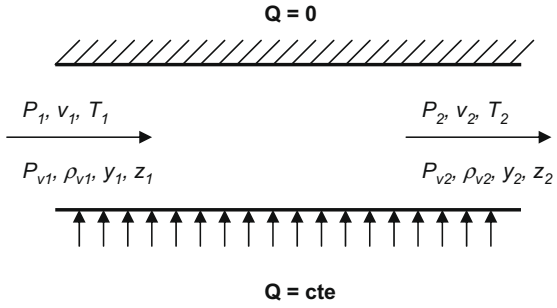

Fig. 1. Schematic overview of the heating of humid air in a duct: parameters which indicate mixture composition should have the same value at the inlet and the outlet.

the inlet and the outlet, otherwise its use would result in a non-existing mass diffusion flux.

Based on the inlet conditions, the outlet conditions for this example are calculated using the ideal gas law and using the conservation laws for mass, energy and momentum. Table 1 gives the inlet conditions and the resulting outlet conditions. This example shows that under non-isothermal conditions the difference in vapour density is a poor driving force for mass transport. The water vapour pressure does not remain constant either, although the change is small compared to the change in water vapour density. The small change in water vapour pressure can be attributed to the small deviation from an isobaric condition in the channel. This simple example confirms that the actual driving force for mass transfer is the difference in mass fraction Y or mole fraction Z, two parameters which are only influenced by the composition of the mixture.

The above analysis indicates that if the convective mass transfer coefficient is defined using mass or mole fractions as driving force, a direct relation between the convective mass flux and the process of mass diffusion is expressed, even for non-isothermal, non-isobaric systems. Opposed to this, the definition of the mass transfer coefficient using vapour densities or vapour pressures can result in a driving force for convective mass transfer different from zero while there is no mass diffusion flux.

As both differences in mass and mole fractions represent a good driving force for mass transfer it is interesting to know how mass transfer coefficients defined by these two driving forces are related. Rewriting the convective flux from an expression as function of mass fractions to a function of mole fractions results in Eq. (5) for the case of water vapour transport in air. This equation shows that a constant ratio of h_m^Y and h_m^Z (and thus independence from the value of the driving force) is only possible if the water vapour pressure is much smaller than the total pressure (or if the molar weight of the different species would be equal). According to Ackermann diffusion in a mixture of species with different molar weights results in mass transfer coefficients which have to be corrected for the case of large differences in vapour pressure [9]. To avoid these problems we will focus the analysis on the case of mass transport at low vapour pressures.

$$\begin{aligned} g &= h_m^Y(Y_s - Y_\infty) \\ &= h_m^Y \frac{R_a}{R_v}\left(\frac{1}{1-\left(1-\frac{R_a}{R_v}\right)\frac{P_{v,s}}{P}}\frac{P_{v,s}}{P} - \frac{1}{1-\left(1-\frac{R_a}{R_v}\right)\frac{P_{v,\infty}}{P}}\frac{P_{v,\infty}}{P}\right) \\ &= h_m^Y 0.622\left(\frac{1}{1-0.378\frac{P_{v,s}}{P}}Z_s - \frac{1}{1-0.378\frac{P_{v,\infty}}{P}}Z_\infty\right) \end{aligned} \tag{5}$$

2.3. Adiabatic saturation process

In this section, the behaviour of convective mass transfer coefficients related to the different driving forces is studied based on the theoretical case of an adiabatic saturation process. Adiabatic saturation is a process in which water evaporates into air in a duct in such a way that the air is saturated with water vapour at the outlet. The latent heat necessary for the evaporation is extracted from the air stream only. This results in a temperature decrease of the humid air towards the outlet of the duct. The temperature reached at the outlet, where the air is saturated, is called the adiabatic saturation temperature. To reach steady state conditions water has to be supplied to the system. This is done at the adiabatic saturation temperature itself. Fig. 2 gives an overview of this process. Unlike the wet bulb temperature which depends on geometry, air velocity, supply water temperature and other parameters, the adiabatic saturation temperature is a property of the inlet air–water vapour mixture. However for the normal pressure and temperature range of atmospheric air the adiabatic saturation temperature is closely approximated by the wet bulb temperature [20].

As the necessary latent heat of vaporization is extracted from the air, Chen argued that a relation between the convective heat transfer coefficient h and the convective mass transfer coefficient h_m could be expressed as function of the latent heat and the driving forces for heat and mass transfer [2]. He proposed:

$$\frac{h}{h_m^\rho} = \frac{\left(\rho_{v,sat}(T_{wet}) - \rho_{v,\infty}\right)\Delta H_L(T_{wet})}{(T_\infty - T_{wet})} \tag{6}$$

When comparing this relation with the Chilton–Colburn analogy (Eq. (7)) for different inlet temperatures and humidities a considerable difference was found [2].

$$\frac{h}{h_m^\rho} = \rho C_p Le^{2/3} \tag{7}$$

Table 1
Inlet conditions, outlet conditions and added heat for the case of heating humid air in a duct: indicators for mixture composition should have the same value at the inlet and the outlet.

Property	In	Out
$\dot{m}$ (kg/s)	1	1
v (m/s)	1	1.08
T (K)	300	323.8
Y (kg/kg)	0.05	0.05
ρ_v (kg/m^3)	0.05	0.0463
P_v (Pa)	6930	6927.8
Z (mol/mol)	0.078	0.078
P (Pa)	88,753	88,725
ρ (kg/m^3)	1	0.926
Q (W)	25,000	

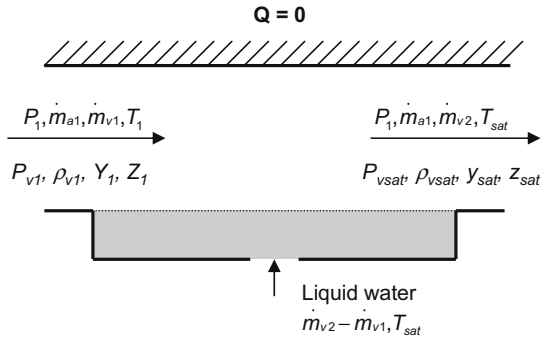

Fig. 2. Schematic overview of the adiabatic saturation process: water evaporates until the air at the outlet is saturated with water.

The relation proposed by Chen will be critically examined and in a second step it will be used to study the effect of varying ambient conditions on the value of the mass transfer coefficient defined by different driving forces. To investigate the reason for the deviation between Eq. (6) and the Chilton-Colburn relation (Eq. (7)), the ratio of the heat and mass transfer coefficient is derived from the governing equations for heat and mass transfer. If the temperature at the water surface can be assumed constant the following equations are found:

$$Q = hA\frac{(T_s - T_{out}) - (T_s - T_{in})}{\ln\left[(T_s - T_{out})/(T_s - T_{in})\right]} \tag{8}$$

$$G = h_m^{\rho}A\frac{(\rho_{v,s} - \rho_{v,out}) - (\rho_{v,s} - \rho_{v,in})}{\ln\left[\left(\rho_{v,s} - \rho_{v,out}\right)/(\rho_{v,s} - \rho_{v,in})\right]} \tag{9}$$

$$Q = -\Delta H_L G \tag{10}$$

where Q and G, respectively, stand for the total heat flow and total mass flow exchanged at the surface.

By substituting Eqs. (8) and (9) in Eq. (10) and by taking into account that the outlet temperature and water vapour density of the adiabatic saturation process are equal to the saturation conditions at the surface, the following equation is obtained:

$$\frac{h}{h_m^{\rho}} = -\Delta H_L\frac{\rho_{v,s} - \rho_{v,in}}{T_s - T_{in}} = -\Delta H_L\frac{\rho_{v,out} - \rho_{v,in}}{T_{out} - T_{in}} \tag{11}$$

If the above equation is equal to the Chilton–Colburn relation (Eq. (7)) then Eq. (12) should be valid. If the Lewis number is one and the latter equation is multiplied with the mass flow rate $\dot{m}$, Eq. (13) is obtained which is an expression of the energy balance in case of constant mass flow rate and density. Hence the relation proposed by Chen equals the Chilton–Colburn relation for a case with constant mass flow rate and density, if the Lewis number is equal to one.

$$\rho C_p Le^{2/3}(T_{out} - T_{in}) = -\Delta H_L(\rho_{v,out} - \rho_{v,in}) \tag{12}$$

$$\dot{m}\,C_p(T_{out} - T_{in}) = -\Delta H_L\frac{\dot{m}}{\rho}(\rho_{v,out} - \rho_{v,in}) \tag{13}$$

If the Lewis number is significantly different from one in an adiabatic saturation process then the air temperature will reach the adiabatic saturation temperature before or after the mass fraction reaches its final value depending on the Lewis number being higher or lower than one. This effect can be seen in Fig. 3. As a result the ratio of local convective heat and mass fluxes is no longer equal to the negative of the latent heat value. The ratio of the total convective fluxes can no longer be used to calculate the ratio of average transfer coefficients because the area through which the flux passes is different for mass and heat transfer. The effect of the Lewis number on the area through which heat or mass is transported is shown in Fig. 3. The validity of Eq. (6) is thus restricted to cases with Lewis number equal to one.

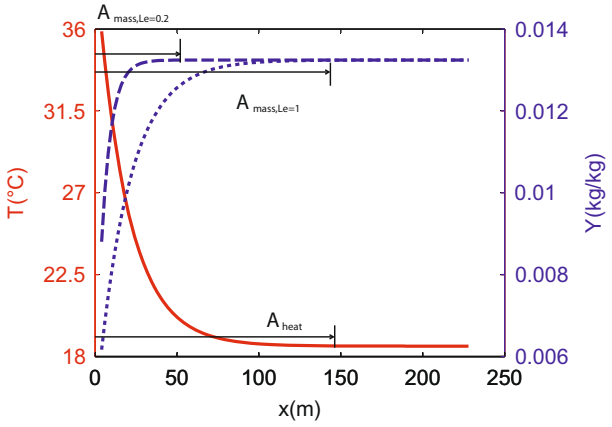

Fig. 3. Evolution of air temperature (——) and mass fraction of water vapour along the flow direction in the adiabatic saturation process. The mass fraction is given for a diffusivity associated with $Le = 1$ (• • •) and with $Le = 0.2$ (▪ ▪ ▪). Under $Le \neq 1$ the heat and mass exchanging surfaces are of different sizes.

Instead of using water vapour density in Eq. (6) it is also possible to use the other driving forces for mass transfer mentioned previously. Under the condition that the Lewis number is one, Eq. (13) changes in Eqs. (14)–(16) for, respectively, mass fraction, mole fraction and water vapour pressure as driving force. The new equations represent the energy balance of the adiabatic saturation process under the conditions that, respectively, the mass flow rate (Eq. (14)), the molar flow rate (Eq. (15)) and both the total pressure and the molar flow rate (Eq. (16)) are constant. Under these conditions the ratio of the heat and mass transfer coefficient can be expressed as a function of the heat of vaporization for the different definitions of h_m.

$$\begin{aligned} &C_p(T_{out} - T_{in}) = -\Delta H_L(Y_{out} - Y_{in}) \\ &\quad\Longleftrightarrow \dot{m}\,C_p(T_{out} - T_{in}) = -\Delta H_L\,\dot{m}(Y_{out} - Y_{in}) \end{aligned} \tag{14}$$

$$\begin{aligned} &\rho C_p(T_{out} - T_{in}) = -\Delta H_L cM_v(Z_{out} - Z_{in}) \\ &\quad\Longleftrightarrow \dot{n}(ZM_v + (1-Z)M_a)C_p(T_{out} - T_{in}) \\ &\quad= -\Delta H_L M_v\,\dot{n}(Z_{out} - Z_{in}) \end{aligned} \tag{15}$$

$$\begin{aligned} &\rho C_p(T_{out} - T_{in}) = \frac{-\Delta H_L}{R_v T}(P_{v,out} - P_{v,in}) \\ &\quad\Longleftrightarrow \dot{n}(ZM_v + (1-Z)M_a)C_p(T_{out} - T_{in}) \\ &\quad= -\Delta H_L\frac{M_v}{P}\,\dot{n}(P_{v,out} - P_{v,in}) \end{aligned} \tag{16}$$

Similarly as described in Section 2.2 for mass diffusion, it appears that vapour density can only be used as a driving force for convective mass transfer under the condition of constant density. The use of vapour pressure as driving force seems restricted to isobaric cases. To investigate this, the ratio of the heat and mass transfer coefficients is calculated for the different driving forces using the latent heat relation for an inlet relative humidity varying between 2% and 40% at three different ambient conditions: 40 °C and 1 atm., 40 °C and 0.8 atm., 70 °C and 1 atm. Under these conditions the driving force for mass transfer and by consequence the evaporation rate are relatively small, which means that the condition of constant mass flow rate or constant molar flow rate in the air is a good approximation.

The results of this analysis are shown in Fig. 4: the dependence of the ratio h/h_m on the ambient conditions is depicted for four different driving forces. Fig. 4a) shows that, as expected, h_m^{ρ} strongly depends on the inlet temperature and inlet pressure but also on the inlet relative humidity. The influence of the temperature and pressure is clear as these two properties strongly affect the density. Also the effect of the relative humidity can be explained by density variations: the relative humidity determines the magnitude of the difference between the inlet temperature and the adiabatic saturation temperature and by consequence of the density difference between the inlet and the surface. Hence a change in relative humidity will change the density variation in the air. Fig. 4b) shows that unlike for h_m^{ρ} the dependence on inlet pressure, temperature and relative humidity of h_m^{Y} is very small. This agrees with the fact that no assumptions were made with regard to the density when defining h_m^{Y}. Fig. 4c) shows the dependence of h_m^{P} on the total pressure. Not withstanding the fact that the adiabatic saturation process itself is isobaric, the value of the total pressure influences the value of h_m^{P}. In Fig. 4d) it can be seen that by using mole fractions instead of water vapour pressures the dependence of the

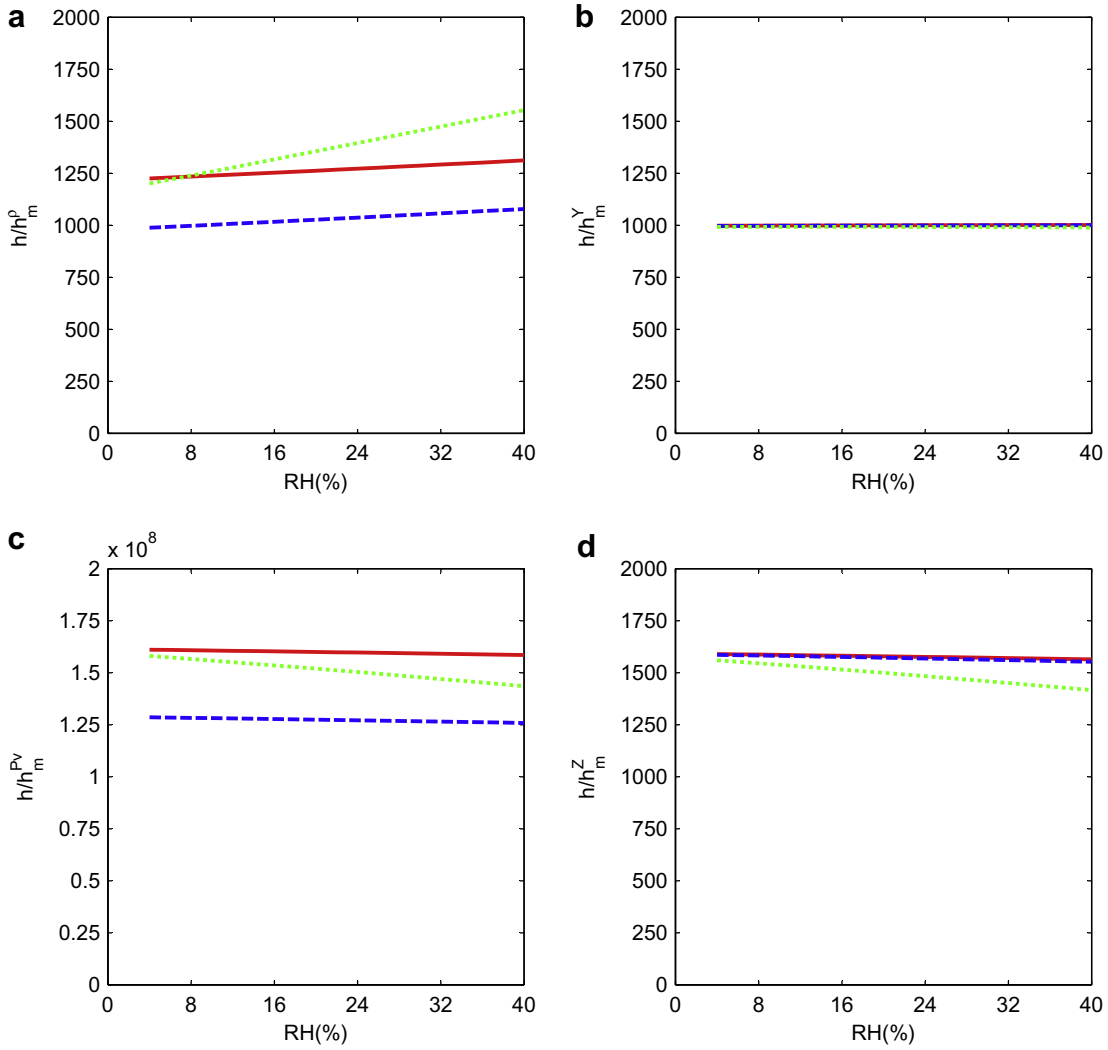

Fig. 4. Ratio of heat and mass transfer coefficient as function of inlet relative humidity for inlet temperature and inlet pressure of 40 °C and 1 atm. (——), 40 °C and 0.8 atm. (- - -), 70 °C and 1 atm. (- - -) in the adiabatic saturation process. The mass transfer coefficient is defined with a driving flux of vapour densities (a), mass fractions (b), vapour pressures (c) and mole fractions (d).

mass transfer coefficient on the total pressure cancels. By increasing the relative humidity at a temperature of 70 °C h_m^Z starts to deviate from the constant value found for the other considered conditions. This behaviour can be explained by considering Eq. (5): at 70 °C an increasing relative humidity will result in increasing values of the vapour pressure which can no longer be considered negligibly small compared to the total pressure (e.g. at 40% RH the ratio of vapour pressure to total pressure is 0.029 for 40 °C while it is 0.123 for 70 °C). Hence the relation between h_m^Z and h_m^Y becomes a function of the vapour pressure and by consequence of the relative humidity.

In general it can thus be stated that use of mass fractions or mole fractions instead of water vapour density or water vapour pressures as a driving force for convective mass transfer leads to mass transfer coefficients which are less dependent on the ambient conditions.

3. Practical application: a realistic evaporation experiment

The objective of this section is to look into the practical consequences of the use of the different convective mass transfer coefficients. This is done by studying a well defined evaporation experiment for laminar and turbulent flow by Iskra [1]. In this experiment h_m^ρ was used to calculate the Sherwood number. Iskra found that h_m^ρ and *Sh* varied with inlet temperature and relative humidity and explained this by the effect of buoyancy.

Using CFD this experiment is simulated for realistic non-isothermal conditions similar to those measured in the experiment and for a case with isothermal conditions. Out of the CFD results *Sh* numbers are calculated using h_m^ρ and h_m^Y. These values are then compared with the experimental findings. Also the influence of temperature on the different *Sh* numbers is examined and the heat and mass transfer analogy is used to compare these *Sh* numbers with well-established heat transfer correlations [21,22].

3.1. Description of the simulated test case

In the considered setup water is evaporated out of a tray into a rectangular duct. The water tray has a length of 600 mm and a width of 280 mm. The duct is 20.5 mm high and has a width of 298 mm. Upstream of the water tray a developing section is present which results in a hydrodynamically developed airflow at the test section (above the water tray). A more elaborate description of the test setup can be found in [1]. In the experiments the inlet temperature was kept more or less constant at a value of about 23 °C and the inlet relative humidity was varied. In a first set of

CFD simulations (adiabatic cases) the inlet temperature is fixed at 23 °C and three different inlet relative humidities are studied: 20%, 40% and 80%. With each different inlet relative humidity a different water surface temperature is associated. This temperature is assumed to be the adiabatic saturation temperature. An overview of the boundary conditions for these adiabatic cases is given in Table 2. In a second set of CFD simulations (non-adiabatic cases) the water surface temperature is no longer equal to the adiabatic saturation temperature: two non-isothermal cases for which the water temperature is lower than the adiabatic saturation temperature and one (nearly) isothermal case are considered. The boundary conditions for these cases are given in Table 3. The Rayleigh numbers for mass transfer ($Ra = GrSc$) associated with the different cases are also mentioned in Tables 2 and 3 and, except for the isothermal case, they fall into the range of experimentally tested conditions [1].

In the test section the hydrodynamically developed air flow has developing boundary layers for heat and mass transfer. To characterize such a developing flow the inverse Graetz number can be used. This represents a dimensionless axial distance and is defined as Eq. (17) in the case of heat transfer and as Eq. (18) in the case of mass transfer.

$$x^* = \frac{1}{Gz} = \frac{x}{D_H RePr} \tag{17}$$

$$x^* = \frac{1}{Gz} = \frac{x}{D_H ReSc} \tag{18}$$

To vary the dimensionless length (x^*) the Re number was changed in a range between 1000 and 2100 for laminar flow and between 4000 and 9320 for turbulent flow. These ranges agree with the range in which the experiments were originally conducted [1].

In the experiments by Iskra mass transfer data was expressed as mean Sh numbers (Sh_m) in function of x^*. On the other hand the correlations given in [21,22] express the heat transfer as local Nu numbers (Nu_x) in function of x^*. The use of the heat and mass analogy will thus result in a relation for Sh_x as function of x^*. The definitions for Sh_x and Sh_m are given in Eqs. (19) and (20).

$$Sh_x = \frac{h_{m,x} D_H}{D} = \frac{g_x D_H}{D\left(\rho_{v,s} - \rho_{v,m}\right)} \tag{19}$$

$$Sh_m = \frac{1}{x}\int_0^x Sh_x dx \tag{20}$$

In case of a constant value of $\rho_{v,s}$ at the surface Eq. (20) can be written as:

$$Sh_m = \frac{\frac{1}{x}\int_0^x g_x dx D_H}{D(\Delta\rho_v)_{\log}} \tag{21}$$

with

$$(\Delta\rho_v)_{\log} = \frac{\left(\rho_{v,s} - \rho_{v,in}\right) - \left(\rho_{v,s} - \rho_{v,m}(x)\right)}{\ln\left[\left(\rho_{v,s} - \rho_{v,in}\right)/\left(\rho_{v,s} - \rho_{v,m}(x)\right)\right]} \tag{22}$$

Table 2
Boundary conditions for the adiabatic CFD cases.

Property	20%RH	40%RH	80%RH
Inlet temperature (°C)	23	23	23
Inlet relative humidity (%)	20	40	80
Inlet mass fraction (kg/kg)	0.003459	0.006929	0.013936
Surface temperature (°C)	11.2	14.7	20.5
Surface relative humidity (%)	100	100	100
Surface mass fraction (kg/kg)	0.008222	0.010315	0.014944
$Ra = GrSc$ (–)	46600	32100	9270

In the given definition of Sh, ρ_v was used as driving force for mass transfer, yet it is also possible to use the other driving forces. In this study both the local as the mean Sh number will be evaluated using vapour densities and vapour mass fractions as driving force.

3.2. CFD settings

The CFD simulations in this paper are performed with the commercial CFD code Fluent 6.2.16. A 3D simulation of the non-isothermal case showed that the flow can be considered two dimensional as the difference between the simulated evaporation rates for 2D and 3D simulations is less than 1%. Hence the choice was made to perform 2D simulations of the test cases in which only the air side is considered. A constant temperature and mass fraction at the water surface are used as boundary conditions. A structured rectangular grid of 15800 elements was used to discretize the duct. A grid independency study based on Richardson extrapolation was performed which proved that the grid independent mass flux at the studied surface was less than 0.63% different from the value simulated with the chosen grid.

As boundary condition for the inlet velocity a fully developed velocity profile was imposed with an average value prescribed by the studied Re number. In case of laminar flow a parabolic profile, characteristic for fully developed laminar flow, was used to model the velocity and in case of turbulent flow initial simulations were performed to determine the fully developed turbulent velocity profile. The inlet temperature and mass fraction are given in Tables 2 and 3. For the turbulent simulation $0.16Re^{-1/8}$ and $0.07D_H$ were used at the inlet as, respectively, turbulence intensity and as turbulent length scale. These values are related to hydrodynamically developed flow [23]. The values of the boundary conditions for temperature and mass fraction at the water surface are given in Table 2. As the water surface is a semi-permeable interface a diffusion flux of water vapour into air results in a mass increase in the airflow. To take this effect into account a mass source was defined next to the water surface proportional to the evaporation rate (standard Fluent assumes the surface to be fully permeable, which means that the mass is kept constant and diffusion of one species into the domain is accompanied by diffusion of the other species out of the domain).

The incompressible ideal gas law was used to calculate the density. This way, both the effect of temperature and mass fraction on the buoyancy are included in the simulation. Constant values for the dynamic viscosity, thermal conductivity and mass diffusivity were used (evaluated at a temperature of 20 °C). The k-omega turbulence model was used in the turbulent cases. The maximum value of $y+$ found in the simulations was 1.57, which means that the near wall turbulence is well captured. The SIMPLE scheme was used for pressure – velocity coupling together with second order upwind differencing schemes. A double precision representation of real numbers was used to reduce round off errors.

3.3. Comparison of CFD simulation and the evaporation experiment

In this section the results of the evaporation experiment by Iskra are compared with the CFD simulation. As the measured Sh numbers are related to the rectangular duct, the hydraulic diameter of the duct was used in the definition of Sh and x^*.

In Fig. 5, the comparison is made between the measured mean Sh numbers and the simulated ones for laminar flow. The Sh numbers were defined using h_m^{ρ}. Fig. 5a) shows the effect of Ra on Sh as measured by Iskra [1] compared with the adiabatic CFD simulations. Unlike the experiments, the adiabatic simulations indicate that there is no effect of Ra on Sh. The same finding was made by Talukdar who also performed a CFD simulation of the experiment

Table 3
Boundary conditions for the non-adiabatic CFD cases.

Property	Isothermal	Non-isothermal (laminar)	Non-isothermal (turbulent)
Inlet temperature (°C)	23.1	23	23
Inlet relative humidity (%)	55	40	40
Inlet mass fraction (kg/kg)	0.009601061	0.006929256	0.006929256
Surface temperature (°C)	23	12	10
Surface relative humidity (%)	50	100	100
Surface mass fraction (kg/kg)	0.008670738	0.008655221	0.007574
$Ra = GrSc$ (–)	1030	45100	50500

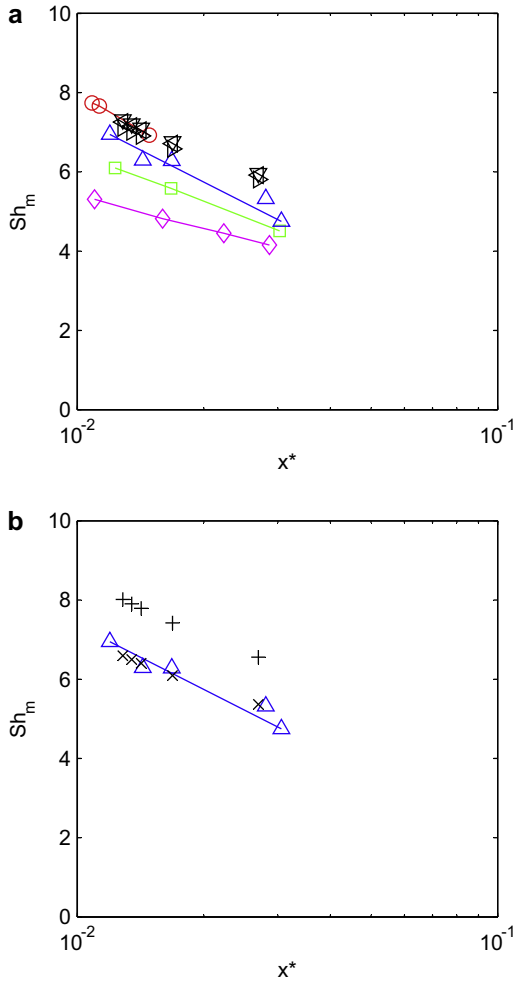

Fig. 5. Effect of density variations on mean *Sh* defined with vapour density as driving force. Laminar flow results for *Sh* as function of dimensionless length. (a) Measurements by Iskra [1] for $6300 < Ra < 7300$ (◊), $16600 < Ra < 17400$ (□), $52200 < Ra < 55700$ (△), $58500 < Ra < 62700$ (○) and CFD simulations for adiabatic evaporation with $Ra = 46600$ (▽), $Ra = 32100$ (◁) and $Ra = 9270$ (▷). (b) Measurements by Iskra [1] for $52200 < Ra < 55700$ (△) and CFD simulations for a non-adiabatic isothermal (+) and non-isothermal case with $Ra = 45100$ (x).

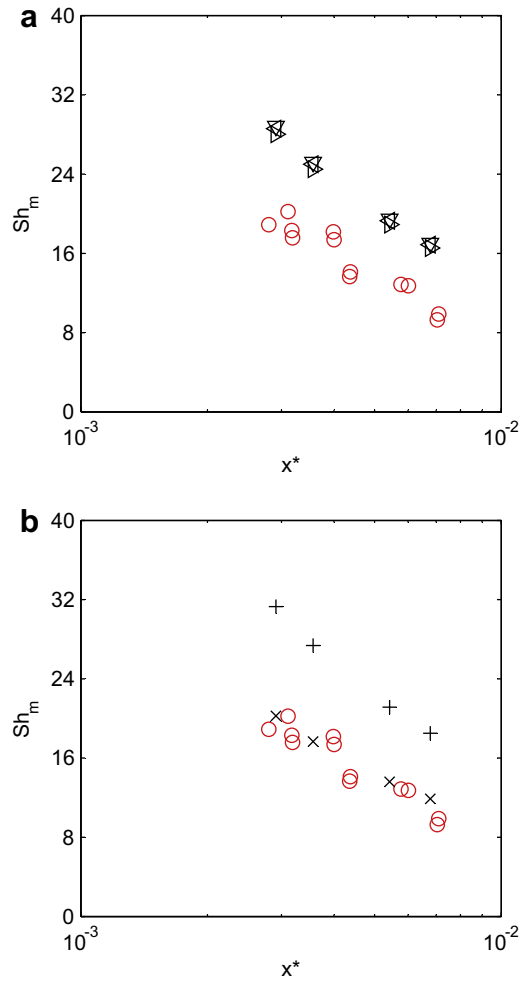

Fig. 6. Effect of density variations on mean *Sh* defined with vapour density as driving force. Turbulent flow results for *Sh* as function of dimensionless length. (a) Measurements by Iskra [1] (○) and CFD simulations for adiabatic evaporation with $Ra = 46600$ (▽), $Ra = 32100$ (◁) and $Ra = 9270$ (▷). (b) Measurements by Iskra [1] (○) and CFD simulations for a non-adiabatic isothermal (+) and non-isothermal case with $Ra = 50500$ (x).

by Iskra [24]. This finding can be physically explained by the fact that the water surface temperature (bottom surface) is lower than the air temperature (and the top surface) which results in a stable stratified flow without free convection. However Fig. 5b) shows that the non-isothermal, non-adiabatic CFD results agree very well with the experiments for the same *Ra* range. Fig. 6 shows that the same findings can be made when experiments and simulations are compared for turbulent flow.

When the *Sh* numbers for the CFD simulation are recalculated with h_m^Y instead of h_m^ρ the $Sh - x^*$ relations for the adiabatic and non-adiabatic cases are converted into approximately the same curve. This phenomenon is observed for both laminar as turbulent flow (Fig. 7.). This confirms that *Ra* exerts no influence on *Sh* for this setup and indicates that the different *Sh* numbers found by Iskra for the different inlet relative humidities are possibly not caused by flow phenomena like increased buoyancy forces but might be an artefact of the use of water vapour densities as driving force for convective mass transfer. There might be some other effects which explain this apparent dependence of *Sh* on *Ra* found in the experiments (e.g. the effect of the Gukhman number [25–

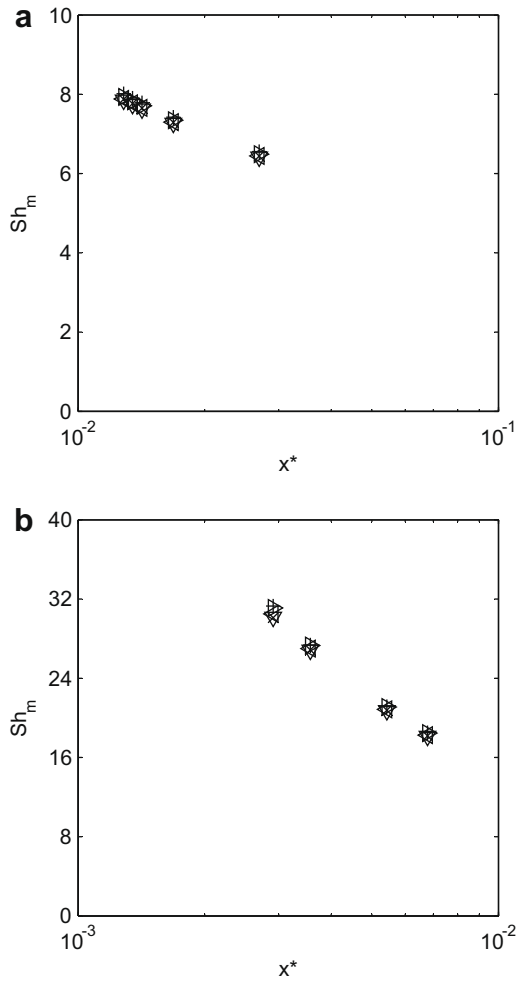

Fig. 7. Effect of density variations on mean *Sh* defined with vapour mass fraction as driving force. CFD results of *Sh* as function of dimensionless length for adiabatic evaporation with *Ra* = 46600 (▽), *Ra* = 32100 (◁) and *Ra* = 9270 (▷) and for a non-adiabatic isothermal (+) and a non-isothermal case (×) in case of (a) laminar flow and (b) turbulent flow.

26]), but it is clear that the use of mass transfer coefficients defined with vapour density as driving force is a possible source of error.

The CFD simulations confirm the findings on the dependence of h_m^ρ on density made in the section on the adiabatic saturation process. Hence if values of h_m^ρ are used in non-isothermal conditions they will only result in an accurate prediction of the mass flux under exactly the same conditions as those they were originally measured for. Under different conditions their use will result in under or over predictions of the mass flux.

3.4. Comparison of CFD simulation and convective transfer coefficient correlations

Heat transfer correlations for a geometry similar to the simulated experiment can be converted into mass transfer correlations using the heat and mass analogy. It is checked how well the converted correlations agree with the CFD simulations of the evaporation experiment for the different definitions of the convective mass transfer coefficient.

The analogous heat transfer case which best represents the evaporation experiment and for which sufficient data was found is the case of hydrodynamically developed flow with a developing thermal boundary layer between two parallel plates of which one is adiabatic and the other is isothermal. Such a case is described by Shah and London for laminar flow and by Sakakibara for turbulent flow [21,22]. Unlike (Figs. 5–7) which give the mean *Sh* number over the entire mass exchanging surface as function of the dimensionless total length of this surface, the correlations proposed by Shah and London and by Sakakibara express the local *Nu* number as function of a dimensionless position along this surface. The turbulent correlation is applicable to a flow with *Re* 10,000 (*Re* related to the hydraulic diameter of the parallel plate). The CFD simulation of *Re* 1000 (*Re* 1073 related to the parallel plate) and *Re* 9320 (*Re* 10,000 related to the parallel plate) are compared with respectively the laminar and turbulent correlation.

Fig. 8a) shows that for the laminar isothermal case the agreement between CFD and the correlation is excellent for local *Nu* and *Sh* numbers (*Sh* based on h_m^ρ). For the non-adiabatic, non-isothermal case the agreement remains excellent for *Nu*, yet for *Sh* a deviation between the correlation and CFD simulation occurs (Fig. 8b). However, when h_m^Y is used to define *Sh*, the CFD results coincide with the laminar correlation for both the isothermal as the non-isothermal case (Fig. 8c). Also for the turbulent case a perfect agreement between CFD and the correlation is found for *Nu* and for *Sh* based on h_m^Y (Fig. 9).

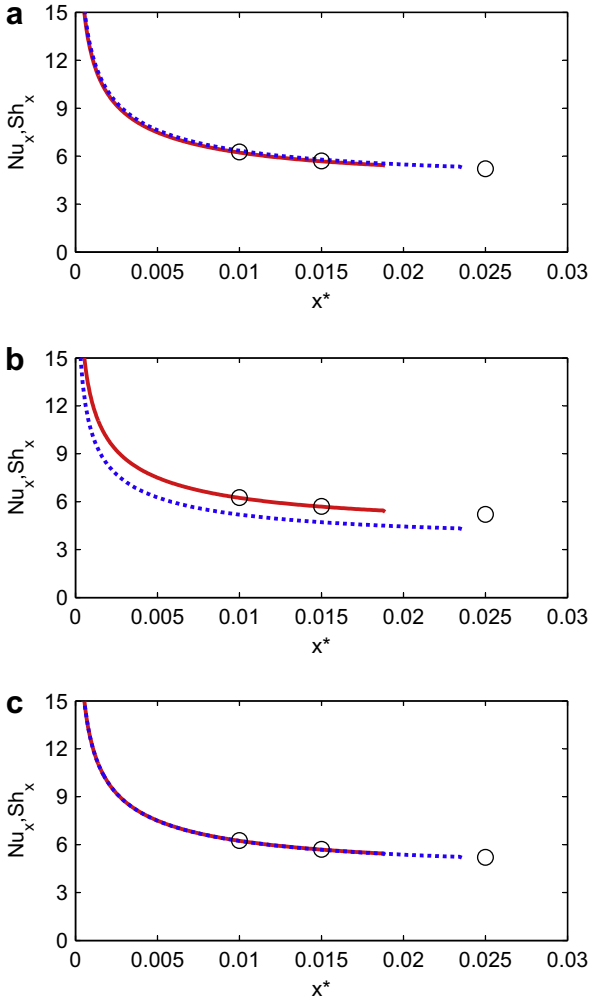

Fig. 8. Comparison of the CFD prediction of local *Nu* (——) and local *Sh* (▪ ▪ ▪) with the correlation of Shah and London (○) [21] for laminar flow. (a) Non-adiabatic, isothermal case with *Sh* defined using h_m^ρ, (b) non-adiabatic, non-isothermal case with *Sh* defined using h_m^ρ, (c) non-adiabatic, non-isothermal case with *Sh* defined using h_m^ρ.

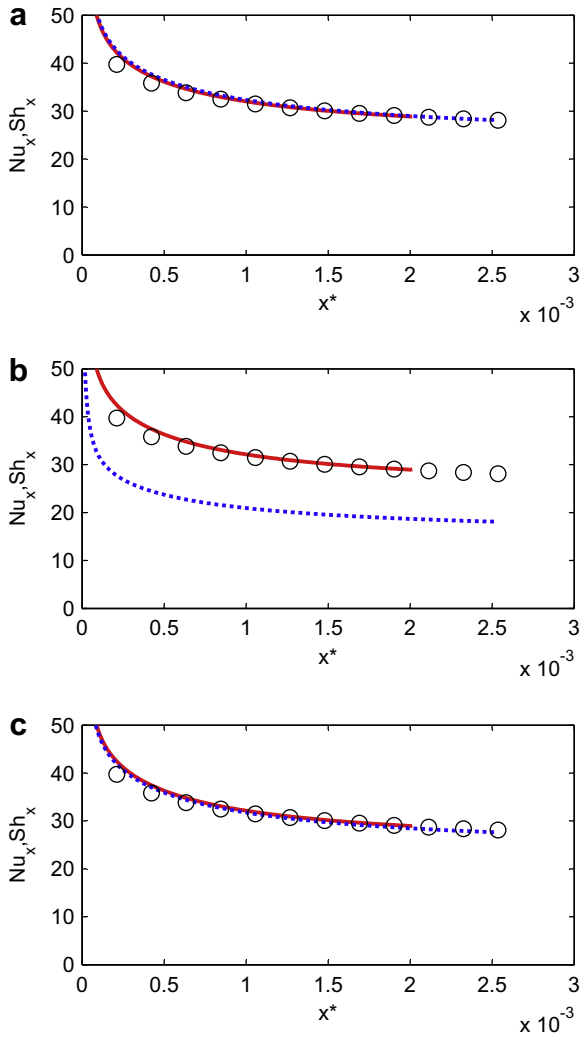

Fig. 9. Comparison of the CFD prediction of local *Nu* (——) and local *Sh* (▪ ▪ ▪) with the correlation of Sakakibara and Endo (○) [22] for turbulent flow. (a) Non-adiabatic, isothermal case with *Sh* defined using h_m^ρ, (b) non-adiabatic, non-isothermal case with *Sh* defined using h_m^ρ, (c) non-adiabatic, non-isothermal case with *Sh* defined using h_m^ρ.

A remarkable finding of the above analysis is the applicability of the heat transfer correlations to mass transfer without having to correct for a Lewis number different from one (in this study $Pr = 0.72$; $Sc = 0.58$). It should although be noted that *Nu* and *Sh* numbers are not directly exchangeable as they depend on a dimensionless length x^* which has a different definition for heat and for mass transfer (Eqs. (18) and (19)). This could be considered as a correction in function of *Le*. A second point of attention is the fact that in the considered cases the vapour pressures are small and that in case of high vapour pressures extra difficulties can arise when correlating *Nu* and *Sh* due to the increased effect of semi-permeable surfaces, different molar weights for the diffusing species, etc. Nevertheless when converting heat transfer correlations it is very important to use the obtained *Sh* number to calculate mass transfer coefficients based on mass fractions and not on vapour densities, unless the considered case is isothermal. This confirms again the superiority of h_m^Y compared to h_m^ρ. The excellent agreement between CFD and the considered correlations also proves the quality and the correct implementation of the CFD study.

4. Conclusions

In this paper, the different definitions of mass transfer coefficients are investigated by both theoretical analysis as by CFD simulation. The theoretical analysis showed that convective mass transfer coefficients related to vapour pressure as driving force are only applicable to isobaric systems and should be corrected by the total pressure when used under a different ambient pressure.

The use of convective mass transfer coefficients related to vapour density is only allowed under condition of constant density. If this condition is not fulfilled the values of h_m^ρ will show a dependence on ambient conditions such as temperature, relative humidity and pressure. Hence if h_m^ρ is used in non-isothermal conditions an accurate prediction of the mass flux will only be possible under exactly the same ambient conditions as those for which the mass transfer coefficients were originally determined.

It is thus recommended to use mass transfer coefficients related to mass fractions as driving force. Using this definition the mass transfer coefficients are quasi independent of the ambient temperature, relative humidity and total pressure. An extra advantage of this definition of the mass transfer coefficient is that it allows to directly convert heat transfer correlations for *Nu* into mass transfer correlations for *Sh* for the case of dilute gas mixtures.

Acknowledgement

The results presented in this paper have been obtained within the frame of the FWO Project B/05836/02 funded by the FWO-Flanders (Research Fund Flanders) and of the SBO IWT 050154 Project, funded by 'IWT Vlaanderen', the Institute for the Promotion of Innovation by Science and Technology in Flanders. This financial support is gratefully acknowledged.

References

[1] C.R. Iskra, C.J. Simonson, Convective mass transfer coefficient for a hydrodynamically developed airflow in a short rectangular duct, Int. J. Heat Mass Transfer 50 (11–12) (2007) 2376–2393.
[2] X.D. Chen, S.X.Q. Lin, G.H. Chen, On the ratio of heat to mass transfer coefficient for water evaporation and its impact upon drying modeling, Int. J. Heat Mass Transfer 45 (21) (2002) 4369–4372.
[3] S.B. Nasrallah, P. Perre, Detailed study of a model of heat and mass-transfer during convective drying of porous-media, Int. J. Heat Mass Transfer 31 (5) (1988) 957–967.
[4] A. Erriguible, P. Bernada, F. Couture, M.A. Roques, Modeling of heat and mass transfer at the boundary between a porous medium and its surroundings, Drying Technol. 23 (3) (2005) 455–472.
[5] C. Debbissi, J. Orfi, S. Ben Nasrallah, Evaporation of water by free or mixed convection into humid air and superheated steam, Int. J. Heat Mass Transfer 46 (24) (2003) 4703–4715.
[6] W.R. Foss, C.A. Bronkhorst, K.A. Bennett, Simultaneous heat and mass transport in paper sheets during moisture sorption from humid air, Int. J. Heat Mass Transfer 46 (15) (2003) 2875–2886.
[7] A. Kaya, O. Aydin, I. Dincer, Numerical modeling of heat and mass transfer during forced convection drying of rectangular moist objects, Int. J. Heat Mass Transfer 49 (17-18) (2006) 3094–3103.
[8] W. Masmoudi, M. Prat, Heat and mass-transfer between a porous-medium and a parallel external flow – application to drying of capillary porous materials, Int. J. Heat Mass Transfer 34 (8) (1991) 1975–1989.
[9] G. Ackermann, Wärmeübergang und molekulare Stoffübertragung im gleichen Feld bei groben Temperatur- und Partialdruckdifferenzen, VDI-Forschungshefte 382 (1937) 1–16.
[10] H. Janssen, B. Blocken, J. Carmeliet, Conservative modelling of the moisture and heat transfer in building components under atmospheric excitation, Int. J. Heat Mass Transfer 50 (5-6) (2007) 1128–1140.
[11] Z.H. Hu, D.W. Sun, Predicting local surface heat transfer coefficients by different turbulent kappa-epsilon models to simulate heat and moisture transfer during air-blast chilling, Int. J. Refrigeration – Revue Internationale Du Froid 24 (7) (2001) 702–717.
[12] A. Hukka, The effective diffusion coefficient and mass transfer coefficient of Nordic softwoods as calculated from direct drying experiments, Holzforschung 53 (5) (1999) 534–540.
[13] J.S. Lewis, Heat transfer predictions drom mass transfer measurements around a single cylinder in cross flow, Int. J. Heat Mass Transfer 14 (1971) 325–329.

[14] J.P. Schwartze, S. Brocker, The evaporation of water into air of different humidities and the inversion temperature phenomenon, Int. J. Heat Mass Transfer 43 (10) (2000) 1791–1800.
[15] N. Boukadida, S. Ben Nasrallah, Mass and heat transfer during water evaporation in laminar flow inside a rectangular channel – validity of heat and mass transfer analogy, Int. J. Thermal Sci. 40 (1) (2001) 67–81.
[16] W. Chuck, E.M. Sparrow, Evaporative mass-transfer in turbulent forced-convection duct flows, Int. J. Heat Mass Transfer 30 (2) (1987) 215–222.
[17] J.H. Jang, W.M. Yan, C.C. Huang, Mixed convection heat transfer enhancement through film evaporation in inclined square ducts, Int. J. Heat Mass Transfer 48 (11) (2005) 2117–2125.
[18] R.B. Bird, W.E. Stewart, E.N. Lightfood, Transport Phenomena, New York, 1960.
[19] J. Welty, C. Wicks, R. Wilson, G. Rorrer, Fundamentals of Momentum, Heat and Mass Transfer, fourth ed., John Wiley & Sons, New York, 2001.
[20] M.J. Moran, H.N. Shapiro, Fundamentals of Engineering Thermodynamics, third ed., New York, 1998.
[21] R.K. Shah, A.L. London, Laminar Flow Forced Convection in Ducts, 1978.
[22] M. Sakakibara, K. Endo, Analysis of heat-transfer for turbulent-flow between parallel plates, Int. Chem. Eng. 16 (4) (1976) 728–733.
[23] Fluent Inc., Fluent user's guide Version 6.2, Fluent Inc., Lebanon, 2005.
[24] P. Talukdar, C.R. Iskra, C.J. Simonson, Combined heat and mass transfer for laminar flow of moist air in a 3D rectangular duct: CFD simulation and validation with experimental data, Int. J. Heat Mass Transfer 51 (11–12) (2008) 3091–3102.
[25] B.M. Smolsky, G.T. Sergeyev, Heat and mass transfer with liquid evaporation, Int. J. Heat Mass Transfer 5 (10) (1962) 1011–1021.
[26] Y. Katto, H. Koizumi, T. Yamaguchi, Turbulent heat transfer of a gas flow on an evaporation liquid surface, Bull. JSME 18 (122) (1975) 866–873.